

Response Component Analysis for Sea State Estimation Using Artificial Neural Networks and Vessel Response Spectral Data

Nathan K. Long^{a,b,*}, Daniel Sgarioto^b, Matthew Garratt^a, Karl Sammut^{c,d}

^a*University of New South Wales, Campbell ACT, Australia*

^b*Defence Science and Technology Group, Fishermans Bend VIC, Australia*

^c*Defence Science and Technology Group, Edinburgh SA, Australia*

^d*Flinders University, Tonsley SA, Australia*

Abstract

The use of the ‘ship as a wave buoy analogy’ (SAWB) provides a novel means to estimate sea states, where relationships are established between causal wave properties and vessel motion response information. This study focuses on a model-free machine learning approach to SAWB-based sea state estimation (SSE), using neural networks (NNs) to map vessel response spectral data to statistical wave properties.

Results showed a strong correlation between heave responses and significant wave height estimates, whilst the accuracy of mean wave period and wave heading predictions were observed to improve considerably when data from multiple vessel degrees of freedom (DOFs) was utilized. Overall, 3-DOF (heave, pitch and roll) NNs for SSE were shown to perform well when compared to existing SSE approaches that use similar simulation setups. Given the information-dense statistical representation of vessel motion responses in spectral form, as well as the ability of NNs to effectively model complex relationships between variables, the designed SSE method shows promise for future adaptation to mobile SSE systems using the SAWB approach.

Keywords: sea state estimation, ship as a wave buoy, multilayer perceptron,

*Corresponding author

Email address: nathan.k.long.91@gmail.com (Nathan K. Long)

1. Introduction

The safety and efficiency of seagoing vessels are greatly affected by operational conditions [1]. Due to the relationship between vessel motion and the wave properties that cause them, the ability to estimate wave conditions, such as wave heights, frequencies, and directions, offers a number of major advantages to operators of maritime platforms.

A vessel can modify its route, based on sea state information, to reduce the likelihood of extreme motions and impact loads on the ship. This can help to increase the comfort and safety of crew and passengers onboard, as well as protect cargo and vessel systems from unwanted damage. Further, vessel route optimisation can reduce fuel consumption by traversing calmer waters. For example, by using a dynamic sea state estimation (SSE) system, regions of rough seas could be avoided entirely by investigating the state of the sea ahead of a maritime platform.

One emerging solution to the SSE problem is the use of the ‘ship as a wave buoy’ (SAWB) analogy. The SAWB technique involves establishing the relationship between a vessel’s motion and the causal wave properties [2]. As such, the vessel can be deployed in the sea and its motion responses recorded, then interpreted to estimate the encountered wave conditions. The use of uninhabited surface vessels (USVs) creates platforms which can be deployed in-situ and in real-time for SSE, as well as being dynamically operable.

Researchers often look to nature when solving complex problems or looking for ways to augment existing processes, such as by using biologically inspired machine learning (ML) algorithms. Artificial neural networks (NNs) are simplified representations of the neural connections in the brain, which can be used to map complex relationships between input data and output variables [3].

This paper presents a model-free approach, based on NNs, to define the

relationship between sea states and vessel motions. The NNs were developed to take vessel spectral response data as input, then output wave properties. Specifically, heave, pitch, and roll data was used as input, while significant wave height, mean wave period, and wave heading represent the outputs.

While most other ML-based SSE techniques using SAWB have used raw time-series response data as input [4, 5, 6], it was hypothesised that the use of spectral response information could provide an information dense alternative, with potential for future use in online SSE. As such, 3-DOF vessel response time-series data was simulated for a range of parametric Modified Pierson-Moskowitz (MPM) sea states, then transformed into their power spectral density (PSD) representations to use as input to the designed NNs. Additionally, the total power and forward speed were recorded to accompany the PSD response data to train the SSE models.

Furthermore, a study was conducted into the estimation performance when each DOF response component was used separately, as well as combined 2-DOF models and 3-DOF models, to investigate the relative contributions information from each DOF and various combination makes to the NN-based SSE method. As such, 21 separate NNs for SSE were developed, one for each estimated wave property for the single DOF, combined 2-DOF, and 3-DOF models.

This paper provides a review of background literature on SSE in Section 2, the simulation models, response data transformation, and NN construction methodologies are given in Section 3, results and discussion are presented in Section 4, before concluding remarks are made in Section 5.

2. Background

Several different techniques have been developed to estimate sea states, with some of the most common methods including the use of wave buoys [7], ship-based radar [8], satellite-based remote sensing [9], and an emerging method of using the ‘ship as a wave buoy analogy’ [2].

The most common method of taking sea state measurements is via wave

buoys, floating sensor-mounted platforms [10]. However, they are few and far apart [11], and contain no means of locomotion, thus making them impractical for dynamic operability as part of in-situ applications. Ship-based radar systems solve this problem by allowing measurements to be taken during ocean transit; however, the radar requires frequent calibration, is expensive to install, and interpretation of the radar data is computationally demanding [12].

Satellite-based altimetry encompasses the procedures which involve measuring the time taken for a radar pulse, transmitted from satellite, to reflect from the sea surface and back to the satellite or a separate receiver. The spatial resolution of satellite altimetry, however, is generally quite crude (on the order of $10 - 100km$), as well as having coarse temporal resolutions [13]. Global navigation satellite system (GNSS) geodesy is the triangulation between a GNSS receiver at the ocean surface and global navigation satellites. GNSS geodesy is capable of measuring displacements on the scale of decametres to centimetres [13, 14, 15]. However, its overall complexity and additional noise source from a ship's responses to wave excitation make it less appealing for simple in-situ SSE while at sea, when compared to the SAWB method.

The SAWB analogy applies the principles of wave buoys to ocean-going vessels, where the relationship between a vessel's motion and causal wave properties are modeled. The vessel can then be placed in an unknown sea state and use its motion response information to estimate the causal wave conditions [2]. SAWB shows promise due to its potential for relatively simple, in-situ, near real-time SSEs. While all of the SAWB methods interpret the vessel responses to wave excitation, there are a few key defining features that delineate the methodologies. One major distinction in SAWB is between vessel model-based techniques and model-free approaches.

In model-based SAWB approaches, vessel-dependent transfer functions describe how the wave motion is transferred to vessel responses. Transfer functions can be calculated using three-dimensional (3D) panel codes based on potential wave theory, strip theory, and computational fluid dynamics programs [2]. One of the main assumptions of transfer functions is that moderate wave heights

form a linear relationship with the motion responses. However, this assumption can provide unreliable results in severe wave conditions, where the linear relationship no longer holds, as well as for non-conventional hullforms [16].

Model-free approaches are designed independently to the vessel parameters, instead defining a relationship between input and output data alone. In other words, a connection between known vessel responses to known wave input is created without passing through a physics-based model. Therefore, model-free approaches rely only on data interpretation, usually via ML or a type of filter, circumventing the development of complex transfer functions.

2.1. ML-augmented SSE

The augmentation of SSE using SAWB via the application of ML algorithms has recently gained attention. ML techniques used include quadratic discriminant analysis and partial least square regression [17], as well as deep learning [4, 5, 6, 18].

Arneson, Brodtkorb, and Sørensen [17] separated the SSE problem into wave heading categorization, and wave height and frequency estimation. Wave headings were discretized, representing a classification problem, where quadratic discriminant analysis (QDA) was used to estimate the wave heading classification. Partial least squares regression (PLSR) was then performed for each heading classification to estimate wave heights and periods. The authors transformed vessel response time-series data into frequency-domain response spectra, then took the total power of the spectra to use as input to the QDA and PLSR models. While the authors described their approach as underperforming when compared with model-based approaches, its ability to estimate both low and high sea states highlights one of the major benefits of model-free SAWB. However, fluctuations in the results indicate that further modifications are necessary to improve the robustness of the techniques.

Wave direction is cited as being the most difficult parameter to accurately estimate when using traditional wave estimation methods [4]. Therefore, Mak and Düz [4] focused on improving directional wave estimates by training three

different types of convolutional neural networks (CNNs) to estimate wave headings using ship response data: a CNN for multivariate regression (CNN-REG), a long short-term memory recurrent neural network (MLSTM-RNN) CNN, and a Sliding Puzzle CNN. The authors used 6-DOF time-series response data as input to the CNNs, where data that was input in chronological order was compared to shuffled data, following 5-fold cross-validation. Results showed lower error for the shuffled data, while the MLSTM-RNN CNN and Sliding Puzzle CNN generally outperformed the CNN-REG.

Mak and Düz [5] then tested the performance of their NNs on simulated data. The simulations were conducted using three different ship types, where the same wave input was simulated for each ship in a sea state represented using JONSWAP spectra (a function of significant wave height and mean wave period). The Sliding Puzzle and MLSTM-RNN CNNs were able to estimate the headings with an approximate 1° error for 95% of results, while the CNN-REG was able to estimate the heading with an approximate 4° error, for all ship types, indicating high performance for NN-based SAWB approaches.

A study by Cheng et al. [6] developed a densely connected CNN (dubbed SSENET) to estimate wave heights and directions using ship response data for a vessel with forward speed. Cheng et al.'s method is unique as they introduced a zigzag shaped path for the vessel to follow when collecting response data. The authors grouped the sea states into five wave height categories and separated the wave direction into eight categories, resulting in 40 different sea state combinations. 9-DOF time-series vessel response measurements were used to train the SSENET, taken from 12 real data sets, as well as two simulated data sets. SSENET was able to achieve high accuracy on most of the real data sets, reaching a maximum of 99.61% accuracy when classifying one of them, and an average accuracy of 82.99% for all 12 real data sets. SSENET, further, achieved an 89.81% and 93.46% accuracy for the two simulated data sets. When compared to other NN types, the SSENET results showed the highest accuracy.

Another study by Cheng et al. [18] used vessel response spectrograms as input to the CNNs instead of raw time-series data (SpectralSeaNet). Spectro-

grams describe a combination of both time and frequency information as two dimensional (2D) images. The SpectralSeaNet results were found to outperform a CNN and LSTM trained on raw time-series data, where SpectralSeaNet had an average accuracy of 94%, while the raw time-series CNN had 91% and the LSTM had 79% average accuracy respectively. This study indicates that use of spectral data for NNs designed for SSE shows promise.

Most of the ML-based SSE methods using SAWB have thus far used time-series response data as input [4, 5, 6], though the use of response data in the frequency domain was tested in Arneson, Brodtkorb, and Sørensen’s study [17], as well as combined with time-series data in Cheng et al.’s work [18]. However, no NN has so far been designed for frequency domain input alone.

As response spectra offer a simple, yet information dense, statistical representation of a vessel’s motion, it is hypothesised that this data format may facilitate effective training of NN-based SSE models to estimate wave properties with a high degree of accuracy. Due to the high performance shown when using NNs for time-domain SSE analysis, their applicability to frequency-domain analysis is a logical extension for consideration.

3. Methodology

3.1. Wave Modeling

Ordinary gravity waves are the type of waves of main concern to maritime operations, comprised of both local wind waves and swell waves [19]. Wind waves are generated from the interaction of in-situ wind and the sea surface, while swell waves are caused by winds no longer present, but which disturbed the sea for a sufficient period for the waves to continue propagating. This study focuses only on local wind waves as a proof of concept.

The stochastic nature of the sea surface can be approximated as a composition of multiple sinusoidal waves with varying parameters. Equation 1 defines wave elevation (ζ) as a function of time (t) and uni-directional wave direction (x_w), where ω represents the wave frequency, A_w is the wave amplitude, k_w

is the wavenumber, and ϵ_w is the random phase shift of each of the N_w wave components. The direction of wave propagation is considered relative to north-east-down coordinates.

$$\zeta(x_w, t) = \sum_{n=1}^{N_w} A_{w_n} \sin(k_{w_n} x_w - \omega_n t + \epsilon_{w_n}) \quad (1)$$

Sea states are often characterized by their statistical properties, where three of the most commonly used properties are significant wave height (H_s), mean wave period (T_1), and mean wave heading [20]. Significant wave height represents the average height of the tallest one-third of wave heights, while the mean wave period is the average period, and mean wave heading is the average heading, of all waves measured.

A number of idealised wave spectra have been developed for different wave conditions in order to model the sea surface. The Modified Pierson-Moskowitz (MPM) spectrum was developed to model a fully developed sea [1], parameterized using the significant wave height and zero-crossing wave period (T_z), given in Equations 2 to 4. The zero-crossing wave period can be calculated using the mean period as $T_z = 0.9212T_1$ [21].

$$S_{\zeta_{PM}}(\omega) = \frac{A_{PM}}{\omega^5} \exp\left(\frac{-B_{PM}}{\omega^4}\right) \quad (2)$$

$$A_{PM} = \frac{H_s^2}{4\pi} \left(\frac{2\pi}{T_z}\right)^4 \quad (3)$$

$$B_{PM} = \frac{1}{\pi} \left(\frac{2\pi}{T_z}\right)^4 \quad (4)$$

The wave elevation time-series can then be calculated from a wave spectrum by randomizing the phase components and substituting the wave amplitudes in Equation 1 with those calculated in Equation 5, where S_ζ is the spectral ordinate and $d\omega$ represents the discretized frequency components.

$$A_{w_n} = \sqrt{2S_{\zeta_n}(\omega_n) d\omega} \quad (5)$$

3.2. Ship Model

A Wave glider (WG) is a low-profile USV which uses an underwater glider to propel itself, attached to a float by an umbilical chord, as well as top-mounted

solar panels to power its electronic systems [22]. As such, WGs are powered entirely by renewable energy.

WGs are advantageous for SSE as they have an increased endurance and range when compared with USVs powered by non-renewables. Further, the small size of WGs means that they are more responsive to higher wave frequency waves than larger vessels [16], potentially providing more information from the waves by exploiting these higher frequency motion components. Therefore, it was decided to use a WG as the vessel for this study, with the parameters given in Table 1 (dimensions taken from [22]). However, it was decided to only model the motion of the float to reduce complexity.

Table 1: Wave glider float parameters.

Parameter	Value
Mass (m_π)	$55kg$
Length (L_π)	$2.05m$
Breadth (B_π)	$0.61m$
Draught (T_π)	$0.16m$
Water plane coefficient (C_{wp_π})	0.877
Block coefficient (C_{b_π})	0.731
Displacement (Δ_π)	$150kg$
Transverse metacentric height (GM_{T_π})	$0.264m$

3.3. Vessel Transfer Functions

A vessel has six DOFs related to the motion of its entire body, three translational and three rotational. While 6-DOF motion has been used before to estimate sea states [17, 4, 5], the use of 3-DOFs have been the most common: heave (z_π), pitch (θ_π), and roll (ϕ_π) [23, 24, 25, 16]. Therefore, frequency response functions (FRFs), which are frequency-wise transfers functions that translate wave motion to vessel motion, have been used to calculate heave, pitch and roll motion responses. However, horizontal displacements have been assessed in or-

der to relate the vessel spatially to the wave system coordinates by considering the vessel's forward velocity.

While a vessel's motion for zero forward speed can be calculated directly using the FRFs, when it has a velocity, the motion excitation frequency becomes a function of the wave encounter frequency (ω_e). The wave encounter frequency is a function of vessel speed (U_π) and relative wave heading (μ_h), as calculated in Equation 6.

$$\omega_e = \omega - k_w U_\pi \cos(\mu_h) \equiv \alpha_\Phi \omega \quad (6)$$

The relative wave heading describes the angle between the body-fixed axis of a vessel and the wave-relative direction of wave propagation.

In order to simulate the heave, pitch, and roll motion of the WG to wave excitation, it was decided to use the semi-analytical approach developed by Jensen, Mansour, and Olsen [26]. The series of closed-form expressions developed by [26] only require the following vessel-specific information: vessel length, breadth, draught, displacement, block coefficient, water plane area, and transverse metacentric height (given in Table 1). The vessel is considered as rectangular prism(s) with homogeneous properties. Previous SSE studies using the SAWB approach that have simulated ship responses using the equations derived in [26] include [27, 28, 29, 30].

Equations 7 and 8 are the equations of motion (EOMs) for pitch and heave, which define the basis for their FRFs. The forces from wave excitation are represented as F_0 for heave and G_0 for pitch, while the dimensionless sectional hydrodynamic damping coefficient is shown as Q_π .

$$\left(\frac{2k_w T_\pi}{\omega^2} \right) \ddot{z}_\pi + \left(\frac{Q_\pi^2}{k_w B_\pi \alpha_\Phi^3 \omega} \right) \dot{z}_\pi + z_\pi = A_w F_{0z} \cos(\omega_e t) \quad (7)$$

$$\left(\frac{2k_w T_\pi}{\omega^2} \right) \ddot{\theta}_\pi + \left(\frac{Q_\pi^2}{k_w B_\pi \alpha_\Phi^3 \omega} \right) \dot{\theta}_\pi + \theta_\pi = A_w G_{0\theta} \sin(\omega_e t) \quad (8)$$

It should be noted that WGs can generally only reach maximum speeds between $1m/s$ and $1.5m/s$ [31]. However, it was decided to simulate speeds of up to $5m/s$ so that the SSE results could more easily be extrapolated to other USVs, while it is assumed that such speeds could be attained by future WG

designs (Kessel [31] discusses ways in which the maximum speed of WGs could be increased).

In order to calculate the EOM for roll, the hydrodynamic damping coefficient of the vessel ($B_{\pi_{44}}$) is found by assuming that the vessel is comprised of two prismatic sections of equal draught, but with different breadths and corresponding cross-sectional areas. As such, the vessel model is more complex for roll than heave and pitch, which is required to capture the desired roll characteristics.

Equation 9 gives the EOM for the roll response, where T_{N_ϕ} represents the natural period for roll (from [32]), $C_{\pi_{44}}$ is the restoring moment coefficient, and M_ϕ is the roll excitation moment.

$$\left(\frac{T_{N_\phi}}{2\pi}\right)^2 C_{\pi_{44}} \ddot{\phi} + B_{\pi_{44}} \dot{\phi} + C_{\pi_{44}} \phi = M_\phi \quad (9)$$

Jensen, Mansour, and Olsen’s FRFs provide a simplified representation of the complex interactions between monohull vessels and encountered waves. However, as the vessel response DOFs are assumed to be decoupled, information about DOF cross-spectra information cannot be extracted. Therefore, due to vessel lateral-plane symmetry, differentiation between port and starboard wave headings cannot be made.

The full derivations of Equations 7 to 9 can be found in [26].

3.4. Response Spectra

While other NN-based SAWB SSE techniques used raw time-series data as input, it was hypothesised that response features could be manually extracted by transforming the response time-series data into their PSD representations [33]. PSDs describe how power in the time-series data is distributed across response frequency components, and can be estimated via discrete Fourier transformation (DFT) [34].

However, as discussed by Nielsen [23], a type of smoothing function is desirable when transforming vessel response time-series data into the frequency domain due to the volatility of the derived spectral magnitudes resulting from a DFT. As such, it was decided to use Welch’s method to estimate the PSD of

the vessel response time-series. An in-depth description of Welch’s method is given in [34].

Following experimentation, the *Hann* window was chosen for this analysis, where 15 windows were used for heave and roll transformations, and 13 were used for the pitch transformation. Likewise, the same 50% overlap between windows was selected for heave and roll, while 80% was used for pitch.

The spectral ordinates with the greatest values and their corresponding frequency components were then extracted from the PSDs to be used as input for the SSE NN algorithms. Furthermore, in a similar manner to the study by Arneson, Brodtkorb, and Sørensen [17], the PSD was integrated to obtain the total power of the response spectra to be used as input to the NNs.

Figure 1 gives an example of a PSD for a heave response time-series for 40 minutes. The raw PSD is shown as the thinner green line, the Welch approximation is given as the thicker blue line, and the highest energy components are highlighted as red markers. The left plots give an example of the 30 PSD components using the Welch method with the highest energy, while the right plots show the 80 components with the highest energy.

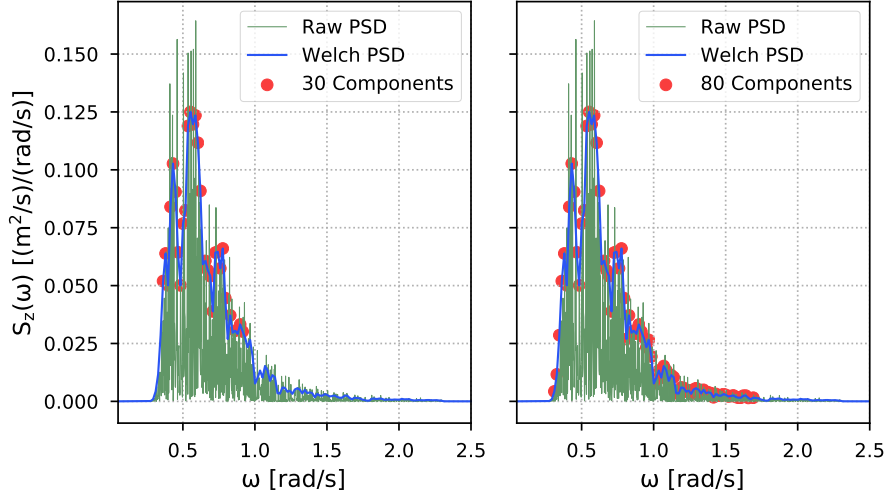


Figure 1: Heave response PSD ($U_\pi = 2m/s$, $\mu_h = 130^\circ$, $H_s = 1.2m$, $T_1 = 8.5$).

The raw PSD is highly volatile, making feature extraction more difficult, while the smoothed PSD derived by Welch’s method provides a good overall approximation of the power distribution. It is hypothesised that the components with the greatest energy of the PSD constitute the most important response information, providing feature-extraction prior to SSE NN training. This reduces the overall complexity required for the NNs, as well as reducing the computational time to train and use the networks, when compared with including all spectral ordinates from the PSDs.

3.5. Sea State Estimation

In order to estimate sea states, vessel motion responses were analysed for different sea and vessel states so that they could be used as input for artificial NNs, which were designed to output the significant wave height, mean wave period, and relative wave heading.

In order to build the NN for SSE, a significant amount of training data was required. Therefore, it was decided to run 48000 simulations of 40 minutes (2400 seconds), broken into 8192 time steps.

For each simulation, an MPM sea spectrum was generated and transformed into a wave system in time and space, where the spectra were comprised of 500 wave frequencies (as in [28]) ranging from $0.5rad/s$ to $2.0rad/s$, then combined with the FRFs from [26] to produce the vessel response time-series.

Table 2 defines the range of each variable tested, which were sampled randomly from uniform distributions.

Table 2: Simulation variable ranges	
Variable	Range
Significant wave height	$0.5m$ to $2.5m$
Mean wave period	$4s$ to $13s$
Relative wave heading	0° to 180°
Vessel speed	$0m/s$ to $5m/s$

It was decided to add noise to the time-series responses to better approximate response measurements using platform onboard sensors. The standard deviations of the noise present in the inertial measurement unit of a waverider buoy [35] were given as $0.01m$ for heave, 0.028° for pitch, and 0.011° for roll. These values were used to generate random noise for each step of the response time-series (assuming a Gaussian distribution for the noise).

3.5.1. Neural Network Architecture

From experimentation, it was determined that 30 PSD components provided sufficient information to estimate significant wave height and mean wave period well, while 80 PSD components performed better when estimating the wave heading. This information was then combined with the values of the PSD total power and vessel forward speed to use as input to the NNs for SSE.

A traditional NN has several layers, where each is comprised of a number of perceptrons (nodes), each of which are associated with an activation function that takes the weighted sum of the previous layer of the network as their input, and produces output for the next layer [3]. In a fully-connected NN, each perceptron in one layer is connected to every perceptron in the next layer. Weights applied to individual connections within the layers are then modified to converge on optimal outputs from the NN overall. Equation 10 defines the activation function of a single perceptron, where x_{p_j} represents the inputs, w_{p_j} are the connection weights, and b_p is the bias.

$$a_p = f \left(\sum_j w_{p_j} x_{p_j} + b_p \right) \quad (10)$$

A multi-layer perceptron (MLP) is a simple feedforward NN, a form of supervised ML which can be used for both regression and classification problems. An MLP was used as the NN for SSE because it enables feature extraction to be completed before being input into the model, requiring a less complex architecture to define the relationship between input and output data. In this case, the NNs take response data and vessel speed as input and produce a wave property (H_s , T_1 , or μ_h) as output.

Separate NNs were designed to input 1-DOF, 2-DOF, and 3-DOF responses. Figure 2 shows the structure of the three different network types. The 1-DOF NN structure is outlined using a solid line, where *input 1* and *input 2* were defined for the spectral ordinates and associated frequency components, while *input 3* contains the vessel speed and response PSD total power. The PSD ordinates and frequencies were concatenated, forming the first *branch* of the NN, then passed to the first hidden layer. The output from this single hidden layer was then concatenated with *input 3*, together comprising the NN *trunk*, which was then passed to another hidden layer, before outputting one of the sea state properties in the final layer.

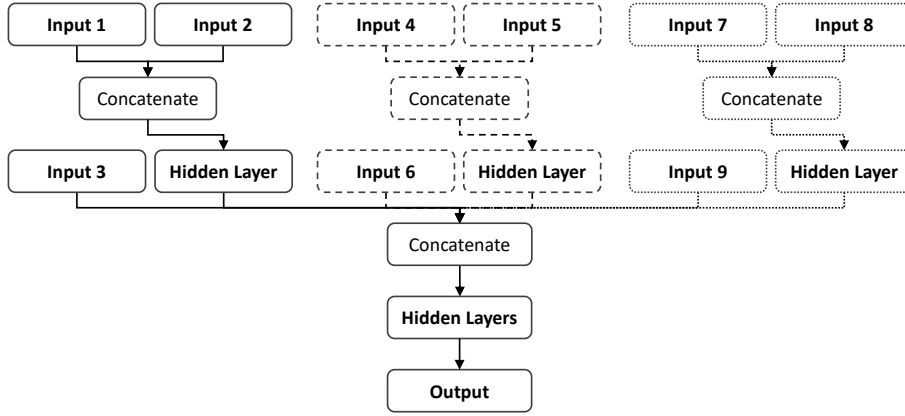


Figure 2: NN structure for 1-DOF (solid line), 2-DOF (dashed line), and 3-DOF (round-dot line) data.

The 2-DOF network is comprised of both the 1-DOF structure and the second branch of the model, comprised of *input 4*, *input 5*, and *input 6*, outlined with a dashed line. The PSD ordinates and frequencies for a second DOF were concatenated then passed to a hidden layer, before being concatenated with the total power of the PSD, vessel speed, and data from the first DOF and passed through the network trunk. Similarly, the 3-DOF model is comprised of the 1-DOF and 2-DOF structures, as well as the third branch outlined with a dotted

line and comprised of *input 7*, *input 8*, and *input 9*, then passed through the same processes as the 1-DOF and 2-DOF models.

For example, a 1-DOF model would take either heave, pitch, or roll response data as input, then output the significant wave height, mean wave period, or wave heading. The 2-DOF variant would then take heave and pitch, for example, and 3-DOF design would take all three DOFs.

The *rectified linear unit* activation function (ReLU) was used for each layer, while the *Adam* optimizer was used to find the best set of node connection weights to map the input data to the desired output, and a *mean square error* loss function was implemented to improve the model fitness.

Separate NNs were trained for each combination of response DOF and sea state property (H_s , T_1 , and μ_h) in order to investigate the sea state information which could be extracted from the different response components.

All of the NN configurations are given in Appendix A. Following experimentation, it was found that network architectures for H_s and T_1 estimation were optimal using the same configurations for the 1-DOF, 2-DOF, and 3-DOF models (given in Table A.8), while the network architectures for μ_h were optimal using an alternative configuration (seen in Table A.9). All of the networks used a single hidden layer with 16 nodes in the branches (to combine the spectral ordinates and frequencies), as well as same number of training epochs (100) and loss rate (0.001). Generally, more network connections were required as additional DOFs were added to the NNs. Further, more nodes were necessary for the NNs used to estimate μ_h , likely due to the fact that more PSD components were used as input to the μ_h networks, so a greater number of connections could better capture the extra information.

It was chosen to perform *k-fold cross-validation* to ensure there was no (or minimal) overfitting or selection bias in model [36]. K-fold cross-validation splits the data into two sets, training data and validation data (here a split of 80/20% was used), then *folds* the data set k_{cv} times (for an 80/20 split, $k_{cv} = 5$). Training and validation is repeated until every sample in the data has been used exactly once in the validation data set. The performance variance of the

model can then be used as a metric to understand the variation in the model's fit, where a lower variance indicates a better fit.

3.5.2. Performance Metrics

Root mean square error (RMSE) and the coefficient of determination (R^2) were selected as performance metrics for the NN models. RMSE represents the sample standard deviation of the difference between the predicted and actual values, where a higher weighting is placed on greater errors, and its units are the same as the predicted variable's units [37]. R^2 is a metric of how well the model fits the data, where a value of 0 represents a model which does not fit the data at all, and a value of 1 represents a perfect fit [37]. Equations 11 and 12 are examples of RMSE and R^2 for significant wave height, where \hat{H}_s is the predicted height, H_s is the actual height, and \bar{H}_s is the average height. The numerator in Equation 11 calculates the prediction residuals ($e_R = \hat{H}_{s_i} - H_{s_i}$), which gives the difference between the predicted value and true value, and can be used to assess how well the data fits the model [37].

$$RMSE = \sqrt{\frac{\sum (H_{s_i} - \hat{H}_{s_i})^2}{N}} \quad (11)$$

$$R^2 = \frac{\sum (\bar{H}_s - \hat{H}_{s_i})^2}{\sum (H_{s_i} - \bar{H}_s)^2} \quad (12)$$

In this case, the trained models were evaluated using a set of test data, 10% of the original data set (4,800 samples), split before the training and validation data sets were split (34,560 and 8,640 samples, respectively).

4. Results and Discussion

4.1. Response Component Analysis

4.1.1. Significant Wave Height

The performance of the network configurations presented in Table A.8 for the different component models when used to estimate H_s are given in Table 3.

The estimation performance for H_s of pitch and roll alone were shown to be quite similar; however, the performance of heave was almost an order of magnitude less than both pitch and roll in terms of RMSE, with a 100 % better (doubled) model fitness (R^2). Heave alone had an R^2 value of 0.990, implying a very close fit of the model to the data, with an average RMSE of only $5.83mm$. When heave was combined with pitch, the NN estimation error only slightly reduced, with heave and roll showing similar performance to heave alone. Pitch and roll together were capable of improved estimation performance; however, still with an RMSE nearly double that of the ‘heave only’ variant’s performance. Therefore, as expected, it can be concluded that heave is the DOF most closely related to wave height for a vessel of similar size to the WG. The models were also found to have little variation between cross-validations, implying little overfitting or selection bias.

Table 3: SSE NN component model performance for H_s .

Response(s)	RMSE Avg.	RMSE Std.	R-Squared Avg.
Heave	$5.83mm$	$0.192mm$	0.988
Pitch	$38.5mm$	$0.464mm$	0.485
Roll	$38.4mm$	$0.743mm$	0.486
Heave + Pitch	$5.51mm$	$0.097mm$	0.990
Heave + Roll	$5.85mm$	$0.070mm$	0.988
Pitch + Roll	$10.1mm$	$0.505mm$	0.966

When considering the residual error distributions for each component NN model for significant wave height estimation (see Figure B.6), the errors associated with the models using heave were found to be slightly worse for greater values of \hat{H}_s , which was also present for the pitch and roll model (although with greater spread). This implies that the models tended to overestimate H_s . The 1-DOF pitch and roll models both saw a steady increase in error as their H_s predictions increased, before reducing again, showing the greatest errors associated with H_s estimations between $1m$ and $2m$, indicating that the models were

underestimating moderate seas, and overestimating smaller seas.

4.1.2. Mean Wave Period

Table 4 presents the results for T_1 estimations using the network architectures given in Table A.8. The NN models for all of the response components were found to perform well, with less variation found between the NNs than for H_s . Heave was shown to be the single DOF which could be used to extract the most information to estimate T_1 , with pitch being second. The combination of both heave and pitch had the lowest errors and best model fit, with an average RMSE of 0.228s and an R^2 value of 0.991. The models all had low RMSE standard deviations, demonstrating that there was little overfitting or selection bias.

Table 4: SSE NN component model performance for T_1 .

Response(s)	RMSE Avg.	RMSE Std.	R-Squared Avg.
Heave	0.368s	0.018s	0.944
Pitch	0.573s	0.023s	0.928
Roll	0.708s	0.021s	0.877
Heave + Pitch	0.228s	0.022s	0.991
Heave + Roll	0.294s	0.042s	0.985
Pitch + Roll	0.401s	0.021s	0.973

The residual distributions for the different mean wave period estimation models (given in Figure B.7 in Appendix B) all had similar shapes, except those without heave which had a greater spread. As expected, the model for heave and pitch showed the least spread with few outliers, and the model for heave and roll showed the second best performance. Greater errors were associated with estimates closer to the centre of the T_1 range than the limits of the range for the roll-only model, which indicates that the NNs underestimated mean periods for moderate seas and overestimated in smaller seas (as seen previously in the results for estimated wave height \hat{H}_s).

4.1.3. Wave Heading

The performance results for each of the μ_h component models (described in Table A.9) are given in Table 5. The models were able to estimate wave headings with relatively high accuracy. Heave alone performed the worst of all models trained, achieving an average RMSE of 18.90° and R^2 of 0.852 (averaged across the 5 k-folds). Roll also performed similarly. However, when roll was paired with pitch, the best estimation results were achieved, with an average RMSE of only 8.40° and R^2 of 0.973. The standard deviations of the RMSE varied considerably, with heave alone showing the greatest selection bias and/or overfitting.

Table 5: SSE NN component model performance for μ_h .

Response(s)	RMSE Avg.	RMSE Std.	R-Squared Avg.
Heave	18.9°	1.13°	0.852
Pitch	10.5°	0.195°	0.956
Roll	18.3°	0.732°	0.866
Heave + Pitch	8.88°	0.473°	0.970
Heave + Roll	12.8°	0.157°	0.935
Pitch + Roll	8.40°	0.221°	0.973

A number of patterns can be seen in the residual distributions for the wave heading estimations for each component model (shown in Figure B.8). For heave alone, the greatest errors are generally estimated around beam sea. This is similar to what was seen for the significant wave height and to a lesser extent mean wave period estimations, with the limits of the wave property range being underestimated and overestimated. However, the greatest outlying errors for most of the models increased in magnitude as they approach head and following sea estimations. This shows that at times the models would estimate head seas as following seas, and vice versa. This can be explained by the similar motion responses induced by the same wave input using the transfer functions for a

vessel in head and following seas for both pitch and roll.

4.2. 3-DOF Models

Finally, the three vessel response DOFs, heave, pitch, and roll, were combined into a single NN to estimate the wave conditions.

The results from the k-fold cross-validation for the 3-DOF models are given in Table 6. As expected, the inclusion of all of the data led to best performance of the models.

Table 6: 3-DOF NN model performance.

Metric	H_s	T_1	μ_h
RMSE Avg.	5.38mm	0.171s	7.21°
RMSE Std.	0.116mm	0.006s	0.411°
R-squared	0.990	0.995	0.980

The 3-DOF H_s model did not see a large increase in performance when compared with the heave and pitch model. The average RMSE reduced to 5.38mm, with a standard deviation of 0.116mm, and an average R^2 value of 0.990. The similar performance could indicate that similar information was extracted from pitch and roll to estimate H_s .

The T_1 estimation performance was, however, improved more considerably when using all of the vessel response data, with an average RMSE of 0.171s and standard deviation of 0.006s, and an average R^2 of 0.995. The closest performance was achieved with the model trained on the heave and pitch data. This indicates that the information extracted from each DOF was considerably different from each other when responding to varying T_1 .

The μ_h estimator experienced some improvement in estimation performance when heave was included, compared to only pitch and roll, but with a lower average RMSE and slightly greater R^2 value. However, this came at the cost of a greater RMSE standard deviation, meaning that there was a greater variation in model performances between k-fold validations.

The residual plots for the 3-DOF wave estimation NNs are presented in Figures 3 to 5. Each of the models show similar patterns to those of the best performing 2-DOF models.

Figure 3 demonstrates a general trend towards larger error for greater H_s estimations, while the 3-DOF T_1 residuals in Figure 4 show that the model is biased towards overestimating T_1 values.

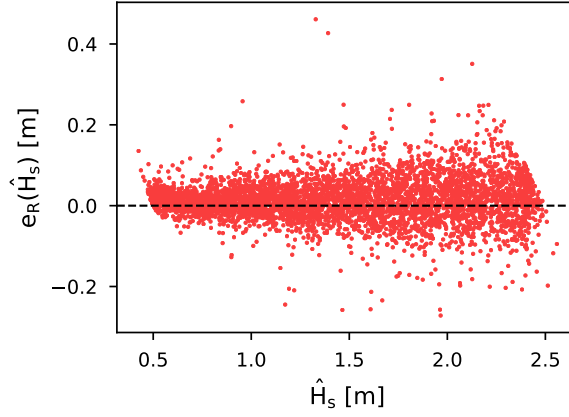


Figure 3: Residual plot for 3-DOF H_s estimations with distribution histogram.

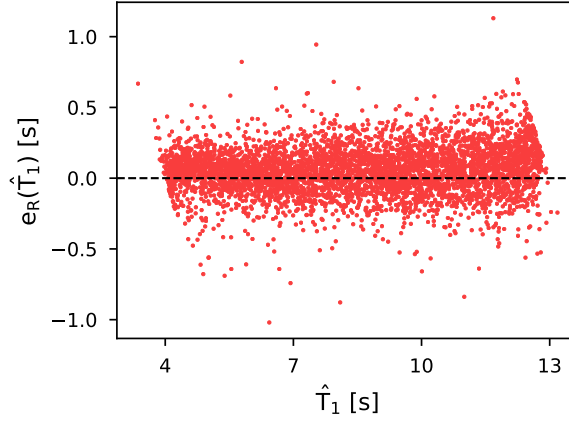


Figure 4: Residual plot for 3-DOF T_1 estimations with distribution histogram.

In Figure 5 it can be seen that the estimations have the greatest accumulation of errors about beam sea. The model is, therefore, tending to incorrectly

estimate the vessel as being in beam seas more frequently than in head or following seas. As seen with the μ_h component model estimations, the outlying greatest errors are seen closer to head and following sea, with the model occasionally mistaking the vessel as being in opposing wave headings.

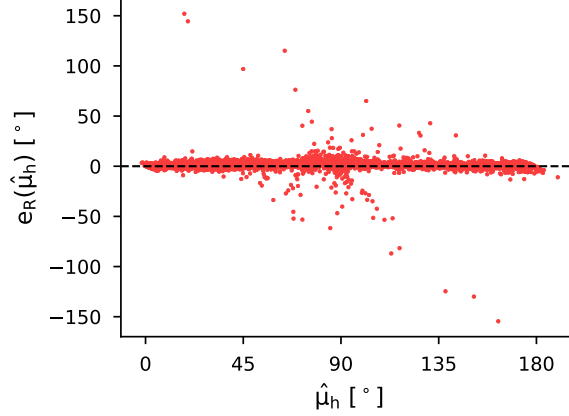


Figure 5: Residual plot for 3-DOF μ_h estimations with distribution histogram.

As a point of comparison with one another, the RMSE for μ_h as a ratio of the range of μ_h values tested was 4.01%. The ratio of RMSE to range for H_s was 2.69%, and the ratio for T_1 was 1.90%. Therefore, the relative estimation performance was best for T_1 and worst for μ_h . However, a comparison with results obtained from other studies provides a better insight into the relative performance of the SAWB-inspired SSE procedure presented here.

4.2.1. Results Comparison

A wide variety of SSE studies using SAWB have been undertaken, where results for the SSEs are presented in many different ways. In order to critically evaluate the results from the described SSE approach, two previous studies providing similar results metrics have been selected for direct comparison.

The study by Arneson, Brodtkorb, and Sørensen [17] is one of the only other ML-based SAWB approaches that uses spectral data to train SSE models (rather than time-series data), and uses similar metrics to this study for presenting the

results. The authors simulated their wave input using a parametric JONSWAP spectrum, using QDA to estimate a wave heading classification and PLSR to then estimate significant wave height and peak wave period. Differences in the approach presented in this paper from the one presented in [17] include analysis of the cross-spectra, resulting in full 360° wave heading estimation, simulating rougher sea states, and 6-DOF responses were used as input. Further, Arneson, Brodtkorb, and Sørensen only used the total power of response spectra as SSE model input. Therefore, their model has been compared using only their results for comparable sea states, while their wave heading angle errors have been compared to the equivalent wave heading errors found in this study. Further, the errors associated with peak wave period were compared with the errors associated with mean wave period using the designed approach.

Hinostroza and Soares [25] developed a model-based approach to SSE using SAWB, which estimated significant wave height and peak wave period for a parametric JONSWAP spectrum, as well as wave heading (within a 180° range). The authors utilized genetic algorithms to calibrate inverse transfer functions which mapped the heave, pitch, and roll responses to the wave spectrum. Hinostroza and Soares [25] tested their method using two different ship types via simulation, as well as via experimentation. The simulation results from the smaller vessel are compared with the developed methodology, while 2 out of 8 cases were omitted as they simulated rough sea states outside the range used for this study.

Table 7 compares the findings from [17] and [25] with the developed 3-DOF SSE NNs.

Table 7: SSE NN performance comparison.

Study	Sig. Wave Height	Wave Period	Wave Heading
	RMSE	RMSE	RMSE
Long et al. 2022	5.38mm	0.171s	7.21°
Arneson et al. [17]	60mm	1.5s	4°
Hinostroza and Soares [25]	23mm	1.1s	9°

When examining the RMSE values for significant wave height, it can be seen that the methodology designed in this work achieved a result that was more than an order of magnitude more accurate than Arneson, Brodtkorb, and Sørensen’s [17], while the RMSE of Hinostroza and Soares [25] was approximately four times greater than for this study. Similarly, the wave period RMSE values for this study were found to be considerably lower than for both [17] and [25]. The results for estimated wave headings, however, were found to be more accurate using Arneson, Brodtkorb, and Sørensen’s classification method than the designed method, while Hinostroza and Soares’s methodology showed slightly worse performance. It should be noted that the results from the work reported here comprised of 4800 instances, while there were only five comparable results from [17] and six from [25]. Further, the relative ship geometries used in the compared SSE methodologies [17, 25] could have an effect on the estimation performance.

Overall, the NN models for SSE designed during this research show promising results when compared with similar approaches. With further development, there is potential for the described methodology to be expanded upon for performance augmentation and possible future implementation in physical systems.

In the future, a number of extensions could be made to this study. Firstly, more complex vessel dynamic and transfer function models should be used which do not assume decoupling between DOFs so that the cross-spectra can be analysed to differentiate between port and starboard wave headings. Secondly, the

networks could be evaluated using model-scale testing data under controlled conditions. Thirdly, the PSD analysis procedure could be further optimized and experimented with to improve SSE performance. Finally, NNs can be tested for a greater range of conditions by using a simulation model capable of capturing non-linear behaviours associated with rougher sea states, thereby improving the robustness of the model and estimations.

5. Conclusion

A new methodology for estimating sea states has been developed, which harnesses the benefits of ML as an alternative to fine tuning physics-based models. Artificial neural network models trained using heave, pitch, and roll vessel response data have been shown to be able to estimate significant wave heights, mean wave periods, and relative wave headings effectively for idealized sea states (within the given constraints). The information which could be extracted from each motion response has been analysed, with results showing a strong correlation between heave responses and significant wave height estimates, whilst the accuracy of mean wave period and wave heading predictions were observed to improve considerably when data from multiple vessel degrees of freedom was utilized. Mean wave period was estimated with the highest accuracy, while wave heading was estimated with the lowest accuracy, with pitch found to be the motion component which best estimated wave heading. Overall, the neural networks trained using 3-degree-of-freedom (heave, pitch and roll) motion for sea state estimation were shown to perform well when compared to existing approaches that use similar simulation setups, indicating that vessel spectral response information can be used for neural network-based sea state estimation.

References

References

- [1] T. I. Fossen, *Environmental Forces and Moments*, John Wiley & Sons, Ltd, 2011, Ch. 8, pp. 187–225. doi:10.1002/9781119994138.ch8.

- [2] U. Nielsen, A concise account of techniques available for shipboard sea state estimation, *Ocean Engineering* 129 (2017) 352–362. doi:10.1016/j.oceaneng.2016.11.035.
- [3] A. K. Jain, Jianchang Mao, K. M. Mohiuddin, Artificial neural networks: a tutorial, *Computer* 29 (3) (1996) 31–44. doi:10.1109/2.485891.
- [4] B. Mak, B. Düz, Ship as a wave buoy: Estimating relative wave direction from in-service ship motion measurements using machine learning, in: *ASME 2019 38th International Conference on Ocean, Offshore and Arctic Engineering*, 2019, pp. 0–12. doi:10.1115/OMAE2019-96201.
- [5] Ship As a Wave Buoy: Using Simulated Data to Train Neural Networks for Real Time Estimation of Relative Wave Direction, Vol. Volume 9: Rodney Eatock Taylor Honoring Symposium on Marine and Offshore Hydrodynamics; Takeshi Kinoshita Honoring Symposium on Offshore Technology of International Conference on Offshore Mechanics and Arctic Engineering. doi:10.1115/OMAE2019-96225.
- [6] X. Cheng, G. Li, A. L. Ellefsen, S. Chen, H. P. Hildre, H. Zhang, A novel densely connected convolutional neural network for sea state estimation using ship motion data, *IEEE Transactions on Instrumentation and Measurement* (2020) 1–1doi:10.1109/TIM.2020.2967115.
- [7] L. F. Bosart, W. A. Sprigg (Eds.), *The Meteorological Buoy and Coastal Marine Automated Network for the United States*, The National Academies Press, Washington, DC, 1998. doi:10.17226/6108.
- [8] W. Huang, X. Liu, E. W. Gill, Ocean wind and wave measurements using x-band marine radar: A comprehensive review, *Remote Sensing* 9 (12). doi:10.3390/rs9121261.
- [9] K. Yu, C. Rizos, A. G. Dempster, GNSS-based model-free sea surface height estimation in unknown sea state scenarios, *IEEE Journal of Selected Topics*

- in *Applied Earth Observations and Remote Sensing* 7 (5) (2014) 1424–1435.
doi:10.1109/JSTARS.2013.2293371.
- [10] V. J. Cardone, B. T. Callahan, H. Chen, A. T. Cox, M. A. Morrone, V. R. Swail, Global distribution and risk to shipping of very extreme sea states (vess), *International Journal of Climatology* 35 (1) (2014) 69–84.
doi:10.1002/joc.3963.
URL <https://rmets.onlinelibrary.wiley.com/doi/abs/10.1002/joc.3963>
- [11] Data Buoy Cooperation Panel, Wave Observations (2019).
URL <http://www.jcommops.org/board/wa/Archives?t=dbcp>
- [12] A. H. Brodtkorb, U. D. Nielsen, A. J. Sørensen, Sea state estimation using model-scale dp measurements, in: *OCEANS 2015 - MTS/IEEE Washington*, 2015, pp. 1–7. doi:10.23919/OCEANS.2015.7404402.
- [13] M. A. Morales Maqueda, N. T. Penna, S. D. P. Williams, P. R. Foden, I. Martin, J. Pugh, Water surface height determination with a GPS wave glider: A demonstration in Loch Ness, Scotland, *Journal of Atmospheric and Oceanic Technology* 33 (6) (2016) 1159–1168. doi:10.1175/JTECH-D-15-0162.1.
- [14] M. A. Morales Maqueda, N. T. Penna, I. Martin, J. Guo, P. R. Foden, Sea surface height measurement using a GNSS wave glider, *Geophysical Research Letters* 45 (11) (2018) 5609–5616. doi:10.1029/2018GL077950.
- [15] N. T. Penna, M. A. Morales Maqueda, I. Martin, J. Guo, P. R. Foden, Sea surface height measurement using a GNSS wave glider, *Geophysical Research Letters* 45 (11) (2018) 5609–5616. doi:10.1029/2018GL077950.
- [16] U. Nielsen, A. Brodtkorb, A. Sørensen, Sea state estimation using multiple ships simultaneously as sailing wave buoys, *Applied Ocean Research* 83 (2019) 65–76. doi:10.1016/j.apor.2018.12.004.

- [17] I. B. Arneson, A. H. Brodtkorb, A. J. Sørensen, Sea state estimation using quadratic discriminant analysis and partial least squares regression, *IFAC-PapersOnLine* 52 (21) (2019) 72 – 77. doi:<https://doi.org/10.1016/j.ifacol.2019.12.285>.
- [18] X. Cheng, G. Li, R. Skulstad, H. Zhang, S. Chen, Spectralseanet: Spectrogram and convolutional network-based sea state estimation, in: *IECON 2020 The 46th Annual Conference of the IEEE Industrial Electronics Society*, 2020, pp. 5069–5074. doi:[10.1109/IECON43393.2020.9254890](https://doi.org/10.1109/IECON43393.2020.9254890).
- [19] W. H. Munk, Origin and generation of waves, in: *Proceedings of 1st International Conference on Coastal Engineering*, 1950, p. 1–4. doi:[10.9753/icce.v1.1](https://doi.org/10.9753/icce.v1.1).
- [20] X. Wang, K. Ichikawa, Effect of high-frequency sea waves on wave period retrieval from radar altimeter and buoy data, *Remote Sensing* 8 (9) (2016) 764.
- [21] B. Lantos, L. Márton, *Nonlinear control of vehicles and robots*, Springer Science & Business Media, 2010.
- [22] P. Wang, X. Zhang, D. Wang, X. Guo, W. Lu, X. Tian, A restricted circle based position keeping strategy for the wave glider, *Applied Ocean Research* 97 (2020) 102081. doi:<https://doi.org/10.1016/j.apor.2020.102081>.
- [23] U. D. Nielsen, Estimations of on-site directional wave spectra from measured ship responses, *Marine Structures* 19 (1) (2006) 33 – 69. doi:<https://doi.org/10.1016/j.marstruc.2006.06.001>.
- [24] M. Höfler, T. Höfler, Sea state estimation in the time domain, Ph.D. thesis, Technical University of Denmark and the Royal Institute of Technology (2017).
URL http://www.nor-mar-eng.org/-/media/Sites/NOR-MAR-ENG/education/thesis_examples/Thesis-Michaela-and-Tobias-Hoefler.ashx?la=da&hash=755434C8DD6E5A44657DBBADCE6F2E5D702B74FD

- [25] M. Hinostroza, C. Guedes Soares, Parametric estimation of the directional wave spectrum from ship motions, *The International Journal of Maritime Engineering* 158 (2016) A121–A130. doi:10.3940/rina.2016.a2.356.
- [26] J. J. Jensen, A. E. Mansour, A. S. Olsen, Estimation of ship motions using closed-form expressions, *Ocean Engineering* 31 (1) (2004) 61–85. doi: [https://doi.org/10.1016/S0029-8018\(03\)00108-2](https://doi.org/10.1016/S0029-8018(03)00108-2).
- [27] U. D. Nielsen, R. Galeazzi, A. H. Brodtkorb, Evaluation of shipboard wave estimation techniques through model-scale experiments, in: *OCEANS 2016 - Shanghai*, 2016, pp. 1–8. doi:10.1109/oceansap.2016.7485701.
URL <https://app.dimensions.ai/details/publication/pub.1093950011>
- [28] A. H. Brodtkorb, U. D. Nielsen, A. J. Sørensen, Sea state estimation using vessel response in dynamic positioning, *Applied Ocean Research* 70 (2018) 76–86. doi:<https://doi.org/10.1016/j.apor.2017.09.005>.
- [29] U. D. Nielsen, A. H. Brodtkorb, A. J. Sørensen, A brute-force spectral approach for wave estimation using measured vessel motions, *Marine Structures* 60 (2018) 101–121. doi:<https://doi.org/10.1016/j.marstruc.2018.03.011>.
- [30] U. D. Nielsen, M. Bjerregård, R. Galeazzi, T. I. Fossen, New concepts for shipboard sea state estimation, in: *OCEANS 2015 - MTS/IEEE Washington*, 2015, pp. 1–10. doi:10.23919/OCEANS.2015.7404386.
- [31] R. Kessel, How sea-wave spectra naturally limit the speed of wave gliders, Tech. rep., Seamount Analytics., Ottawa, Canada (2019).
- [32] S. Kruger, F. Kluwe, A simplified method for the estimation of the natural roll frequency of ships in heavy weather, *HANSA International Maritime Journal* 9 (8) (2008) 1–7.
- [33] J. Deng, B. Maass, R. Stobart, Minimum data requirement for neural networks based on power spectral density analysis, *IEEE Transac-*

tions on Neural Networks and Learning Systems 23 (4) (2012) 587–595.
doi:10.1109/TNNLS.2012.2183887.

- [34] O. M. Solomon Jr, PSD computations using Welch’s method, Tech. rep., Sandia National Labs., Albuquerque, NM (United States) (1991).
- [35] D. Gryazin, L. Starosel’tsev, O. Belova, A. Dzyuba, Inertial measurement unit of waverider buoy. development and test results, Gyroscopy and Navigation 7 (3) (2016) 239–246.
- [36] G. C. Cawley, N. L. Talbot, On over-fitting in model selection and subsequent selection bias in performance evaluation, The Journal of Machine Learning Research 11 (2010) 2079–2107.
- [37] A. R. Jones, Probability, statistics and other frightening stuff, Vol. 2, Routledge, 2018.

Appendix A. Neural Network Configurations

Table A.8: H_s and T_1 NN model configurations.

Element	1-DOF	2-DOF	3-DOF
Branch hidden layers	1	1	1
Branch nodes	[16]	[16]	[16]
Trunk hidden layers	2	3	3
Trunk nodes	[16,8]	[16,8,8]	[32,32,16]
Batch size	32	16	16
Epochs	100	100	100
Loss rate	0.001	0.001	0.001

Table A.9: μ_h NN model configurations.

Element	1-DOF	2-DOF	3-DOF
Branch hidden layers	1	1	1
Branch nodes	[16]	[16]	[16]
Trunk hidden layers	2	3	3
Trunk nodes	[32,16]	[32,32,16]	[32,32,16]
Batch size	16	32	32
Epochs	100	100	100
Loss rate	0.001	0.001	0.001

Appendix B. SSE Component Residual Plots

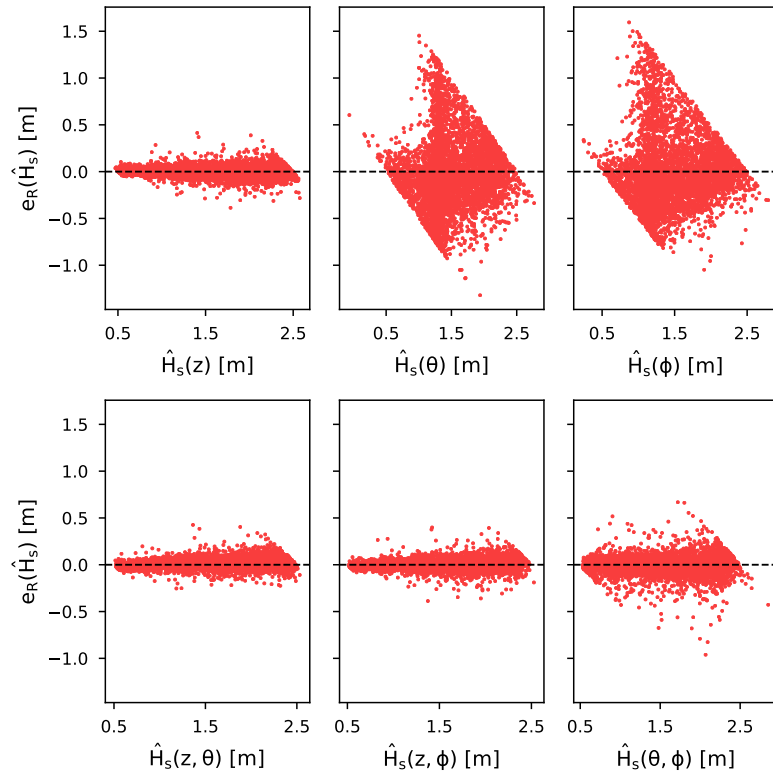


Figure B.6: Residual plots for H_s component estimations.

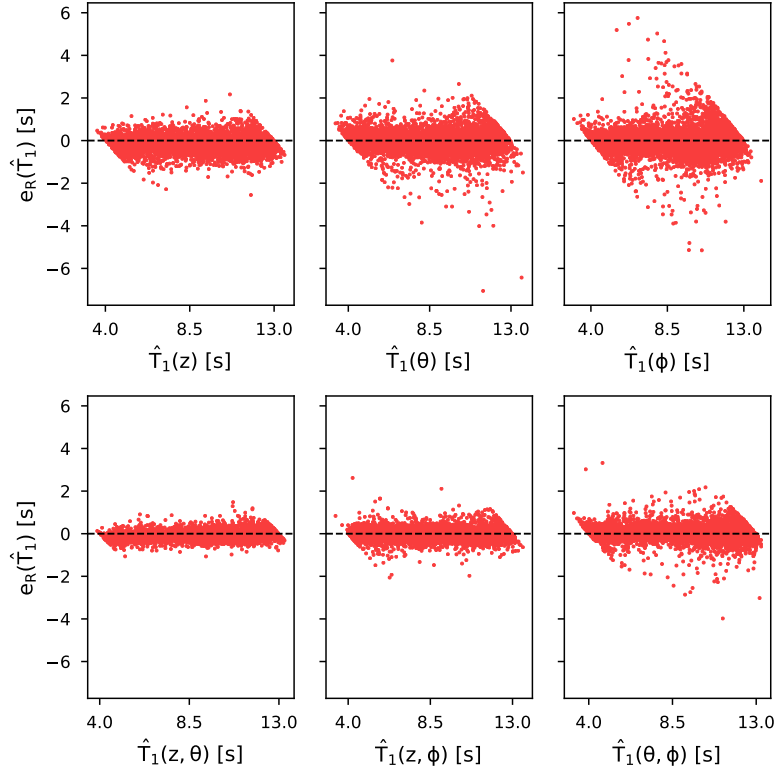


Figure B.7: Residual plots for T_1 component estimations.

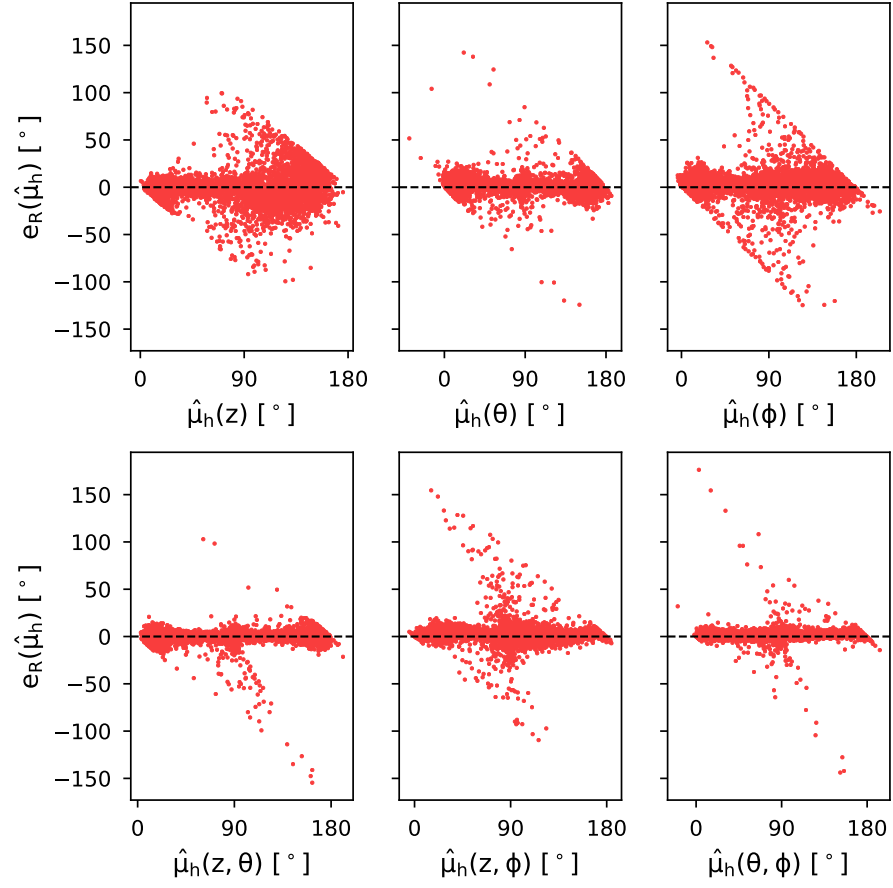


Figure B.8: Residual plots for $\hat{\mu}_h$ component estimations.